On the strain energy distribution of two elastic solids under smooth contact

Y. T. Feng*[,1] Wei Gao†[,2]

[1]Zienkiewicz Centre for Computational Engineering, Swansea University, UK

[2]School of Electromechanical Engineering, Guangdong University of Technology, Guangzhou, China

Abstract

The Hertz contact law for two linear elastic spheres plays a very important role in the discrete element method (DEM). Within the classic Hertz contact theory, the contact strain energy distribution in the two contacting spheres is analytically derived, which states that the ratio between the strain energies stored in the two spheres is solely dependent on their material properties, regardless of their radii. This strain distribution law is generally valid for non-spherical and other contact cases, provided that the two surfaces in contact can be reasonably treated as two elastic half-spaces and that the deformation is small. The independence feature of the law from the contact geometry also greatly facilitates the computation of the contact strain energy stored at particle level. As a direct consequence of this law, the contact point between two particles in DEM could also be determined. The numerical simulations demonstrate good agreement between the theoretical prediction and the numerical results for the tested cases involving spheres and ellipsoids with varying sizes and material properties.

KEYWORDS: Hertz contact theory; Hertz assumptions; Strain energy distribution; Numerical validation

1 Introduction

Hertz theory of contact between two elastic solids is the most important theory in contact mechanics. The Hertz contact law for spheres is the first physically based interaction relationship that provides a simple explicit expression for the normal contact force in terms of the overlap, and thus also plays a very important role in the discrete element method (DEM) [1]. The simple force-displacement form makes it easy to obtain the total contact energy associated with a Hertz contact. However, the rigid nature of the two particles in contact in DEM makes it difficult to compute the contact energy for each particle concerned. To the authors' best knowledge, *there seems no analytical formula available that gives the contact energy for each solid*. Such information on the contact energy distribution, however, may be useful in charactering the overall behaviour of a granular assembly [2], or individual behaviour at particle level.

In this technical note, the contact energy associated with each particle in contact, or contact energy distribution, will be derived based on Hertz contact theory for elastic solids. It will show analytically that based on the Hertz assumptions, the contact energy distribution only

*e-mail: y.feng@swansea.ac.uk

†e-mail: gaowei@gdut.edu.cn

depends on their material properties, regardless of their contact radii or curvatures. The same strain energy distribution law is applicable for general non-spherical contact within the Hertz contact theory.

The extension of the distribution law to non-Hertz contact laws, such as general overlap based power laws and overlap volume based contact laws, is also presented by adopting the assumption that the two contact surfaces in the vicinity/proximity of the contact area are each an elastic half-space, and the conclusion is similar.

From the above development, it is also possible to address another important issue in DEM: how to determine the exact location of a contact point. Such an issue is often ignored or the location is specified in an *ad-hoc* basis. Although within the energy-conserving contact theory framework [5, 6], the contact point is derived for first time in a rigorous manner, its position is not unique for the normal contact point of view, and an additional condition needs to be provided in order to uniquely determine the location. Although such a condition is suggested in [5, 6], it is a pure mathematical exercise and lacks physical justification. With the aid of the current development of the strain energy distribution law, a more rational criterion to determine the contact point will be presented in the present work.

To verify the derived strain energy distribution law, finite element simulations will be used to numerically solve a set of contact problems involving spherical and smooth non-spherical (ellipsoid) solids in contact with different sizes and material properties. The numerical results confirm the theoretical development of the strain energy distribution and also highlights the fact that Hertz theory itself is not exact due to the half-space and small deformation assumptions used.

2 Contact Strain Energy Distribution of Elastic Solids under Hertz Theory

Hertz theory of two elastic solids will be briefly described first. Then the strain energy distribution law will be derived under the Hertz assumptions. First assume that the two solids in contact are linear elastic spheres, while smooth non-spherical contact cases will be discussed in the next section.

2.1 Hertz contact theory of two elastic solids

The main description below is adopted from Chapters 3 and 4 of Johnson's monograph on contact mechanics [3], from which more details can be found.

1). Assumptions

Let R be the equivalent radius of the two solids and a be the radius of the circular contact zone. Hertz theory was derived based on the following four assumptions as stated in [3]:

(i) The two surfaces in contact are continuous and non-conforming: $a \leqslant R$

(ii) The strains are small: $a \leqslant R$

(iii) Each solid can be considered as an elastic half-space: $a \ll R_{1,2}$

(iv) The surfaces are frictionless

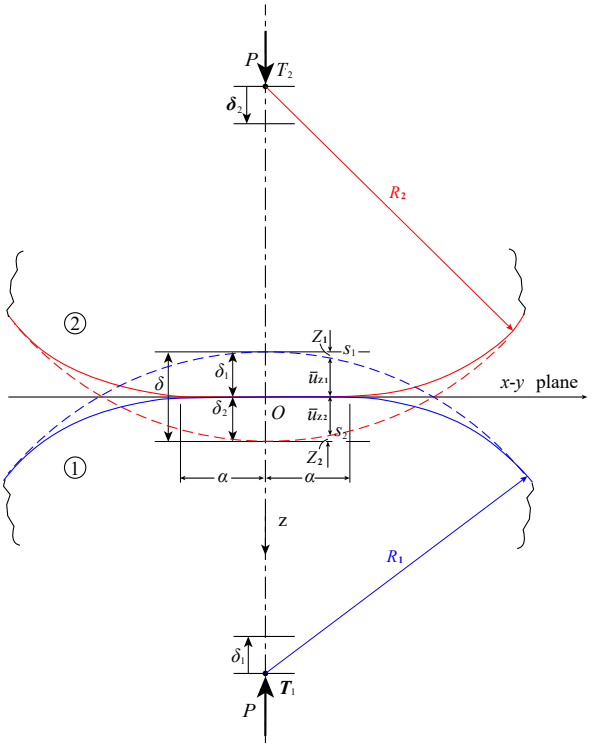

Figure 1: The deformed configurations of two spheres in contact

2). Displacement and pressure distributions

Consider a contact of two spheres as shown in Figure 1, where R_1 and R_2 are the radii of the two spheres; P is the applied compressive force, and δ is the overlap of the two spheres; u_{z_1} and u_{z_2} are the vertical displacements of the two surfaces; r is the radial distance of a point in the contact area to the centre which serves as the origin of a local coordinate system shown in the figure.

Define E_1^ν and E_2^ν to be

$$E_1^\nu = \frac{E_1}{1-\nu_1^2}; \quad E_2^\nu = \frac{E_2}{1-\nu_2^2} \tag{1}$$

The equivalent E of the two solids is expressed as

$$\frac{1}{E} = \frac{1}{E_1^\nu} + \frac{1}{E_2^\nu} \tag{2}$$

The equivalent radius R is defined as:

$$\frac{1}{R} = \frac{1}{R_1} + \frac{1}{R_2} \tag{3}$$

The contact pressure distribution over the contact area can be written as

$$p(r) = p_0 \left[1 - (r/a)^2\right]^{1/2} \tag{4}$$

where $p_0 = p(0)$ is the pressure at the centre of the contact area. The two vertical displacements, u_{z_1} and u_{z_2}, at the contact surfaces satisfy the relationship

$$u_{z_1} + u_{z_2} = \delta - r^2/(2R) \tag{5}$$

Based on the assumption (iii) above, the normal displacement of each solid under the above pressure distribution can be expressed as

$$u_{z_i}(r) = \frac{1}{E_i^\nu}\frac{\pi p_0}{4a}\left(2a^2 - r^2\right), \quad r \leqslant a \quad (i = 1, 2) \tag{6}$$

Consequently the ratio of the two vertical displacements should be

$$\frac{u_{z_1}(r)}{u_{z_2}(r)} = \frac{E_2^\nu}{E_1^\nu} = \frac{1-\nu_1^2}{E_1} \Big/ \frac{1-\nu_2^2}{E_2} \tag{7}$$

i.e., the two displacements differ only by a constant factor that is related to their material properties while independent of their radii/curvatures. Furthermore, the combination of (5) and (7) leads to an alternative but simpler expression for u_{z_i} in terms of δ within the contact zone:

$$u_{z_i} = \frac{E}{E_i^\nu}\left(\delta - \frac{r^2}{2R}\right), \quad r \leqslant a \quad (i = 1, 2) \tag{8}$$

3). The Hertz contact law

The Hertz contact law for linear elastic spheres defines a set of relationships between P, δ, a and p_0. In terms of P, these are

$$a = (R\delta)^{1/2} = \frac{\pi R}{2E}p_0 = \left(\frac{3RP}{4E}\right)^{1/3} \tag{9}$$

$$\delta = \frac{a^2}{R} = \frac{\pi}{2E}(ap_0) = \left(\frac{9P^2}{16E^2R}\right)^{1/3} \tag{10}$$

$$p_0 = \frac{3P}{2\pi a^2} = \left(\frac{6E^2P}{\pi^3R^2}\right)^{1/3} \tag{11}$$

or in the most commonly used $P - \delta$ form in DEM:

$$P = \frac{4E}{3}(a\delta) = \frac{4E\sqrt{R}}{3}\delta^{3/2} \tag{12}$$

2.2 Strain energy distribution

1). Strain energy distribution law for spheres

For a given P or δ, the total strain energy stored in the two contact solids can be readily obtained as

$$S_e = \int_0^\delta P(\delta)\, d\delta = \frac{2}{5}P\delta = \frac{8E\sqrt{R}}{15}\delta^{5/2} = \frac{2}{5}\left(\frac{9P^5}{16RE^2}\right)^{1/3} \tag{13}$$

Next will derive the expression for the strain energy stored in each solid. Based on the fact that the contact pressure is the same for the both surfaces and the corresponding displacements u_{z1} and u_{z2} differ only by a constant factor, it can be readily deduced that the contact strain energies stored in the both solids must differ by the same factor.

Let S_{e1} and S_{e2} be the strain energies stored in the two solids respectively. Their ratio must be

$$\frac{S_{e_1}}{S_{e_2}} = \frac{E_2^\nu}{E_1^\nu} = \frac{1-\nu_1^2}{E_1} \Big/ \frac{1-\nu_2^2}{E_2} \tag{14}$$

or their values can be calculated as a portion of the total contact energy S_e as expressed in (13):

$$S_{e1} = \frac{E}{E_1^\nu} S_e; \quad S_{e1} = \frac{E}{E_2^\nu} S_e \tag{15}$$

The above relationship (14) or (15) is termed *the contact strain energy distribution law*, which indicates that the energy distribution depends only on the material properties and not on their surface radii or curvatures.

In what follows, this contact energy distribution law will be derived in a more concrete manner. To do so, the distributed nature of the contact pressure over the contact area needs to be treated correctly.

Consider one solid involved in contact only and omit the subscript for quantities associated with the solid. Assume that the applied compressive force P increases from 0 to the current value. Given an infinitesimal increase of P by dP, it will cause an infinitesimal change of the vertical displacement $du_z(r)$ over the whole contact area. Then the infinitesimal increase of the strain energy stored in the solid is

$$dS_e = \int_0^a 2\pi p(r) du_z(r)\, r dr \tag{16}$$

Based on (9) to (11), and also (6) or (8), it can be obtained that

$$du_z(r) = \frac{\pi}{3E^\nu} \alpha_a \alpha_p P^{-1/3} dP = \frac{E}{E^\nu} d\delta \tag{17}$$

where

$$\alpha_a = \left(\frac{3R}{4E}\right)^{1/3}, \quad \alpha_p = \left(\frac{9}{16E^2R}\right)^{1/3} \tag{18}$$

Note that $du_z(r)$ is independent of r and further utilise the fact

$$P = \int_0^a 2\pi p(r) r dr \tag{19}$$

it has

$$dS_e = \frac{\pi}{3E} \alpha_a \alpha_p P^{2/3} dP = \frac{E}{E^\nu} P d\delta \tag{20}$$

Hence the total strain energy stored in the solid is

$$S_e = \int_0^P \frac{\pi}{3E^\nu} \alpha_a \alpha_p P^{2/3} dP = \frac{E}{E^\nu} \int_0^\delta P d\delta = \frac{E}{E^\nu} S_e \tag{21}$$

which leads to (15) and further to (14). Thus the strain energy distribution law is formally proved.

2). Strain energy distribution law for non-spherical cases

The above derived strain energy distribution law may be surprising as particle size plays no role in determining the distribution. This result is obtained crucially on the basis that the contact surfaces at the contact area can each be treated as an elastic half-space. Thus it can be concluded that the same distribution law will be applicable for other non-spherical elastic contact cases based on Hertz contact theory, or any case wherever the four Hertz assumptions listed are still valid.

For the Hertz-Mindlin model [4], both normal and tangential deformations occur at the same time but with different dependences of the material properties. The tangential displacement is proportional to $(1-2\nu)/G$ instead of to $(1-\nu^2)/E$ for the vertical displacement as shown in

(6). Thus, the energy distribution ratio of the two strain energies for the tangential direction, S_{e1}^t and S_{e2}^t, is

$$\frac{S_{e1}^t}{S_{e2}^t} = \frac{1-2\nu_1}{G_1} \Big/ \frac{1-2\nu_2}{G_2} \tag{22}$$

which is slightly different from the normal direction ratio (14). The two distributions will only be the same when both materials are the same or the two Poisson's ratios are zero.

If the total contact strain energy can be split into the normal and tangential parts, the two distribution ratios (14) and (22) can be applied separately to the two parts to obtain the strain energy stored in each solid.

For frictional contact cases, the normal distribution law is, strictly speaking, no longer valid as the Hertz assumption (iv) is violated. It is also because the tangential force will induce an additional normal displacement which will alter the normal pressure distribution in a different manner than the frictionless case when the two materials are different (see Chapter 7 in [3] for such a discussion). However, if either the two materials are the same or the tangential frictional force is considered to be independent of the normal contact, the strain energy distribution law can still be regarded as applicable.

3 Strain energy distribution laws for other contact models

Although the above strain energy distribution law is established within Hertz contact theory, similar arguments can be applied to deduce the corresponding energy distribution for other contact models used in DEM, in an approximate fashion. The main difficulty to be overcome stems from the fact that for elastic contact, the Hertz contact model is the only physically correct contact law under the Hertz assumptions.

1) Overlap based contact models

These models, including the most commonly used linear spring model, can be collectively expressed in a general power law form

$$P = k_n \delta^n \tag{23}$$

where k_n is the normal stiffness and $n \leq 1$ is the exponent. Since theses models, except for $n = 3/2$ which is the Hertz model, are not developed based on elastic theory, both pressure distribution and vertical displacement expressions (4) and (6) are no longer valid. Nevertheless, these models can be viewed as a concentrated force P acting on each of the two surfaces which are assumed to be two elastic half-spaces.

Then the vertical displacement of the half-space subjected to the concentrated force P can be expressed as (see Chapter 7 in [3])

$$u_z(r) = \frac{1-\nu^2}{2\pi G}\frac{P}{r} = \frac{1}{\pi E^\nu}\frac{P}{r} \tag{24}$$

Although the vertical displacement at $r = 0$ is infinity, the two vertical displacement fields of the two surfaces again differ only by the same factor as in the Hertz case (6), and thus the same strain energy distribution law (14) is applicable for all these contact models.

Note that the total contact energy S_e can be obtained as

$$S_e = \frac{P\delta}{n+1} = \frac{k_n \delta^{n+1}}{n+1} = \frac{P}{n+1}\left(\frac{P}{k_n}\right)^{1/n} \tag{25}$$

from which the strain energy for each solid can be computed.

2) Contact volume based contact models

For the contact volume based contact models established in [5, 6], the contact pressure in the contact area is a constant. Thus for the contact with two smooth surfaces, the vertical displacement of a half-space subjected to a uniform pressure p over a circular area of radius a has the form [3]

$$u_z(r) = \frac{4(1-\nu^2)pa}{\pi E}\mathbf{E}(r/a) = \frac{4pa}{\pi E^\nu}\mathbf{E}(r/a) \tag{26}$$

where $\mathbf{E}(r/a)$ is the complete elliptic integral of the second kind with modulus (r/a). Again, the two vertical displacement fields differ by the same factor as the Hertz model. The same conclusion can be drawn for the contact area that is not circular. Thus the strain energy distribution law (14) is also valid for the contact volume based contact models if the Hertz assumptions are generally met.

To summarise the above development, the strain energy distribution law appears to be valid for almost all elastic contact models, provided that the two surfaces can be reasonably treated as two half-spaces and that the deformation is small. In particular, its independent feature from the contact geometry greatly facilitates the computation of the contact strain energy stored at particle level. For special cases, where two particles have the same material,

$$S_{e_1} = S_{e_2} \tag{27}$$

or when one solid is rigid, its strain energy $S_e = 0$, as expected.

However, actual contact surfaces are not half-space and small deformation may not be strictly valid. Thus the established strain energy distribution law (14) will not be exact in general cases and its accuracy will depend on the radius or curvature of each surface at the contact area. The smaller (larger) a radius (curvature) is, the lesser accurate the result will be. Nevertheless, the accuracy of this law should be sufficient in the content of DEM where more significant assumptions are often made in both particle shapes and contact interaction laws.

4 The Determination of the contact point

As mentioned in the introduction, no sound theory exists to determine the contact point for a normal contact. The immediate consequence of the derivation of the strain energy distribution law (14) above, or more preciously the displacement distribution relationship (7) is that the contact point can now be uniquely determined.

Refer to Fig. 1, the contact point for the Hertz contact of two spheres should be the origin of the local coordinate system, o. Note that

$$\delta_1 = u_{z_1}(0), \quad \delta_2 = u_{z_2}(0) \tag{28}$$

are the maximum deformations of the two spheres respectively and are related by

$$\delta_1 + \delta_2 = \delta \tag{29}$$

Applying (7) leads to

$$\frac{\delta_1}{\delta_2} = \frac{u_{z_1}(0)}{u_{z_2}(0)} = \frac{E_2^\nu}{E_1^\nu} \tag{30}$$

which yields

$$\delta_1 = \frac{E}{E_1^\nu}\delta, \quad \delta_2 = \frac{E}{E_2^\nu}\delta \tag{31}$$

Thus for a given contact with overlap δ, the contact point o can now be uniquely determined. The same conclusion can be drawn for other contact cases when the Hertz assumptions are generally met.

For the contact of two solids with the same material constants, δ_1 must be the same as δ_2 and therefore the contact point should be the middle point of the maximum overlap.

5 Finite Element Validation of the Strain Energy Distribution Law

In order to validate the strain energy distribution law derived above, three types of contact problems, sphere-sphere, sphere-ellipsoid, ellipsoid-ellipsoid, are numerically solved by the finite element method in this section. To reduce possible numerical modelling errors and increase computational efficiency, all the ellipsoids used are chosen to be axi-symmetrical by setting two principal axes to be the same.

Because all the solids involved are now axi-symmetric, axi-symmetric elements with six nodes are adopted in the FE analysis using the FEM software ABAQUS [7]. All the contact problems are solved by a static procedure with full consideration of *geometric non-linearity*. The surface-to-surface contact algorithm with a "hard" pressure-overclosure relationship is adopted, and the constraint enforcement method, i.e. augmented Lagrange, is employed with the default stiffness with a scale factor 1.0 [7]. The above settings provide the best solution accuracy possible for a given mesh in ABAQUS. Fine meshes are used to discretise the contact region and there are at least 50 elements along the radius direction of each contact zone. Mesh convergence is checked and the final mesh used for each case ensures that no further refinement will improve the numerical results by 0.1%. Due to the geometric symmetry and also the special ways that the loading and boundary conditions are imposed (to be described below), only one quarter of each problem is modelled for computational efficiency.

5.1 Sphere-sphere contact problems

The sphere-sphere contact is considered first. As shown in Fig. 2(a), a compressive displacement δ, which is equal to the overlap, is imposed on the horizontally symmetric plane of the top (small) sphere, while the corresponding symmetrical plane of the bottom (large) sphere is fixed. Initially, the small sphere is just in touch with the large one with zero contact force. Smaller elements are used to discretise the contact region, while relatively larger elements are used for the remaining region. The zoomed mesh around the contact region is illustrated in Fig. 2(b).

To assess the accuracy and validity of the proposed strain energy distribution law, eleven cases with three compressive displacements δ, three Young's moduli E, four Poisson's ratios ν and three radii r are simulated. The radius of the top sphere is fixed to 5mm, while the Young's modulus and Poisson's ratio of the bottom sphere are kept to be 210GPa and 0.3 respectively. The geometric and material parameters, compressive displacements, and element numbers of the spheres for all the cases are listed in Table 1. For illustrative purpose, the vertical displacement distribution of the two spheres in case 2 is shown in Fig. 3.

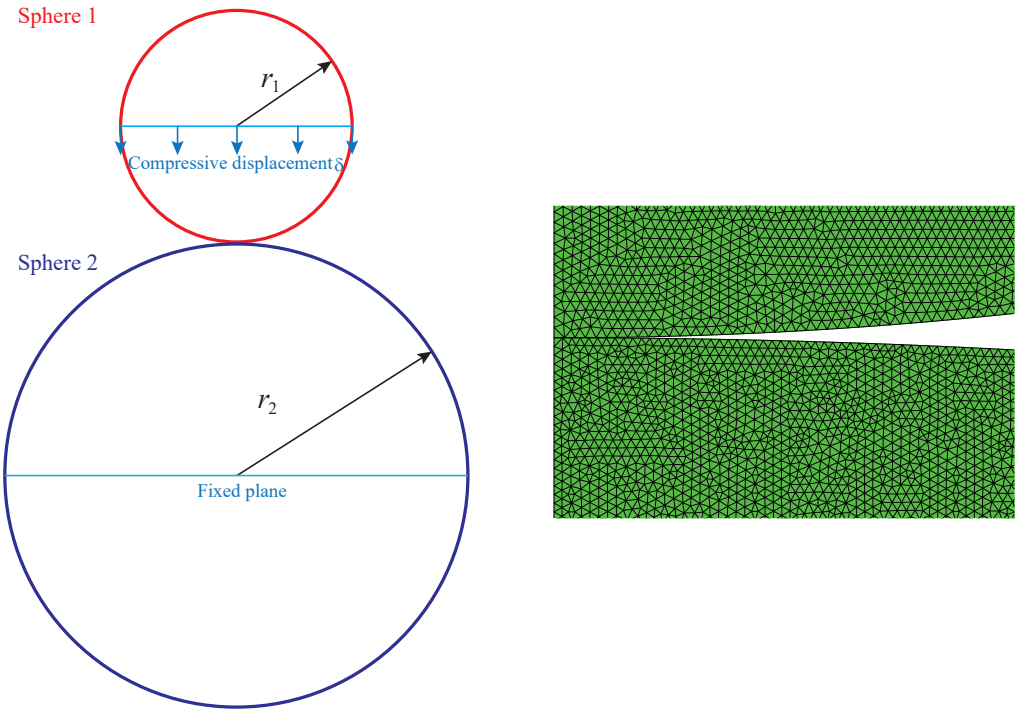

(a) (b)

Figure 2: The sphere-sphere contact problem: (a) geometry, loading and constraint conditions; (b) zoomed mesh in the contact region

Table 1: The geometry and material parameters for sphere-sphere contact cases

Case	δ (mm)	E_1 (GPa)	E_2 (GPa)	ν_1	ν_2	r_1 (mm)	r_2 (mm)	N_1	N_2
1	0.05	210	210	0.3	0.3	5	10	64640	266444
2	0.1	210	210	0.3	0.3	5	10	64640	266444
3	0.2	210	210	0.3	0.3	5	10	64640	266444
4	0.1	105	210	0.3	0.3	5	10	64640	266444
5	0.1	70	210	0.3	0.3	5	10	64640	266444
6	0.1	210	210	0.2	0.3	5	10	64640	266444
7	0.1	210	210	0.1	0.3	5	10	64640	266444
8	0.1	210	210	0.0	0.3	5	10	64640	266444
9	0.1	210	210	0.3	0.3	5	7.5	64640	185424
10	0.1	210	210	0.3	0.3	5	12.5	64640	339407
11	0.1	210	210	0.3	0.3	5	15	64640	474598

N_1 and N_2 denote the element numbers used for spheres 1 and 2, respectively.

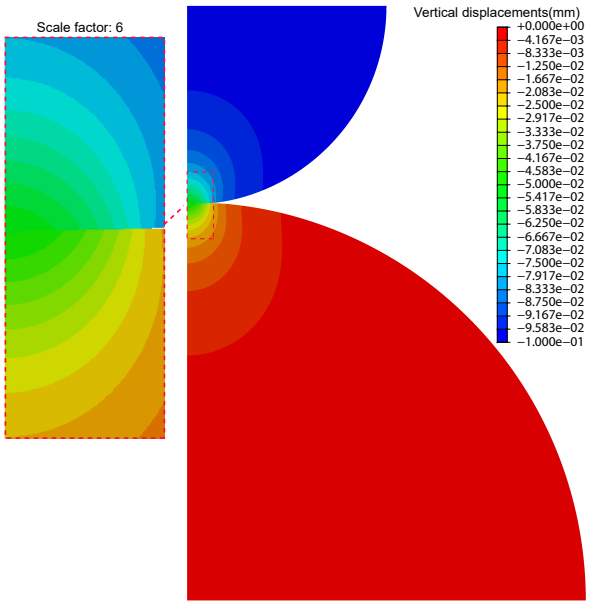

Figure 3: The simulated displacement distribution of the two contact spheres in case 1.

For each case, the strain energies of the two spheres $S_{e_1}^N$ and $S_{e_2}^N$ are evaluated, their ratio $S_{e_1}^N/S_{e_2}^N$ is calculated and compared with the theoretical value S_{e_1}/S_{e_2} given by (14), from which the relative error $e_{12} = (S_{e_1}^N/S_{e_2}^N - S_{e_1}/S_{e_2})/(S_{e_1}/S_{e_2})$ is obtained. All the results are collected in Table 2. As a reference, the computed total contact force for each case is also compared with the Hertz value and the relative error is calculated. These results are also included in the table.

The (absolute) relative errors of the strain energy ratio for all the cases range from 0.7% to 4.0%. This indicates that our theoretical predictions agree well with the numerical simulations in all the simulated conditions, and that the strain energy ratio has a higher accuracy than the Hertz contact force. Examining cases 1, 2 and 3 shows that the energy ratio prediction becomes less accuracy when the maximum compressive displacement increases. This is expected as the increase of the deformation will make the assumption (iii) weaker. Similarly, the increase of the material difference in E between the two spheres will increase the prediction error as evident in cases 2, 4 and 5. In addition, the increase of the size difference between the two spheres also leads to a slightly larger prediction error as shown in cases 9, 10 and 11. However, the effect of enlarging the difference of Poisson's ratio on the error appears to behave differently, as shown in cases 2, 6, 7 and 8, where reducing the Poisson's ratio incrementally adds a positive percentage to the error, so its absolute value is not monotonically decreasing or increasing. No easy explanation can be offered for this effect though.

It should be highlighted that the geometric nonlinearity is fully considered in all the cases and the mesh discretisation error has been reduced to an insignificant level. So errors in the contact force and strain energy show that the Hertz contact theory is not the exact solution but an approximation. Also note a uniformly higher accuracy is obtained for the strain energy distribution than the Hertz contact force. This can be explained as the contact force is the negative gradient of the contact energy [5], and the differentiation will in general reduce the numerical accuracy.

Table 2: The comparisons between numerical and analytical results for sphere-sphere contact cases

Case	P_N (N)	P_A (N)	e_P	S^N_{e1} (mJ)	S^N_{e2} (mJ)	S^N_{e1}/S^N_{e2}	S_{e1}/S_{e2}	e_{12}
1	3240.4	3140.4	3.2 %	31.83	32.35	0.9838	1.0000	-1.6 %
2	9302.5	8882.3	4.7 %	181.16	185.65	0.9758	1.0000	-2.4 %
3	26898.3	25123.0	7.1 %	1033.72	1073.11	0.9633	1.0000	-3.7 %
4	6239.0	5921.5	5.4 %	161.75	83.80	1.9302	2.0000	-3.5 %
5	4696.9	4441.2	5.8 %	136.99	47.58	2.8793	3.0000	-4.0 %
6	8995.6	8644.8	4.1 %	180.40	174.10	1.0362	1.0549	-1.8 %
7	8772.8	8508.3	3.1 %	179.52	166.16	1.0804	1.0879	-0.7 %
8	8627.5	8463.8	1.9 %	178.74	161.33	1.1079	1.0989	0.8 %
9	8850.1	8426.5	5.0 %	172.96	175.70	0.9844	1.0000	-1.6 %
10	9612.2	9194.1	4.5 %	186.75	192.48	0.9702	1.0000	-3.0 %
11	9838.0	9421.1	4.4 %	190.83	197.46	0.9664	1.0000	-3.4 %

5.2 Sphere-ellipsoid contact problem

Fig. 4 shows the set-up of the second contact problem to be used to test the strain energy distribution law, where the top sphere is kept unchanged with the same radius of 5mm, while the bottom sphere in the previous problem is replaced by an ellipsoid with the three principal axes of 10, 10 and 7.5mm. The loading and constraint conditions are imposed in the same way as in the previous problem, and a similar level of mesh discretisation is also used, resulting in 64640 and 210517 elements for the sphere and the ellipsoid respectively. The compressive displacement imposed is fixed to be 0.1mm.

The material property of the ellipsoid is fixed as: Young's modulus 210GPa and Possion's ratio 0.3, while three Young's moduli and three Possion's ratios are chosen for the sphere, resulting in six test cases. Again, for each case, the strain energies of the two solids $S^N_{e_1}$ and $S^N_{e_2}$ are evaluated, their ratio $S^N_{e_1}/S^N_{e_2}$ is calculated and compared with the theoretical value S_{e_1}/S_{e_2} given by (14), from which the relative error e_{12} is obtained. The material properties used in these six cases and the strain energy comparisons are presented in Table 3, which shows that the relative errors are in a similar but slightly lower level as to the previous sphere-sphere contact cases. Note that no contact force comparison is offered as no effort has been put to derive the analytical formula for such a sphere-ellipsoid contact.

Table 3: The material parameters and comparisons of six sphere-ellipsoid contact cases

Case	E_1 (GPa)	ν_1	S^N_{e1}	S^N_{e2}	S^N_{e1}/S^N_{e2}	S_{e1}/S_{e2}	e_{12}
1	210	0.3	193.2577	194.3198	0.9945	1.0000	-0.5 %
2	105	0.3	171.4852	87.14262	1.9678	2.0000	-1.6 %
3	70	0.3	144.7787	49.31208	2.9360	3.0000	-2.1 %
4	210	0.2	192.3510	182.0032	1.0569	1.0549	0.2 %
5	210	0.1	191.3341	173.4979	1.1028	1.0879	1.4 %
6	210	0.0	190.4456	168.2636	1.1318	1.0989	3.0 %

5.3 Ellipsoid-ellipsoid contact problem

In the third ellipsoid-ellipsoid contact problem, the ellipsoid in the previous problem is kept unchanged in both the dimensions and the material property, but the top sphere is replaced by another ellipsoid with three principal axes of 5, 7.5 and 7.5mm. The geometric setting is

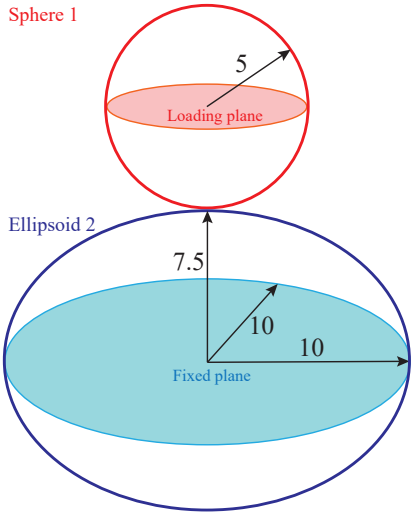

Figure 4: The geometry, loading and constraint conditions of the sphere-ellipsoid contact problem (unit:mm).

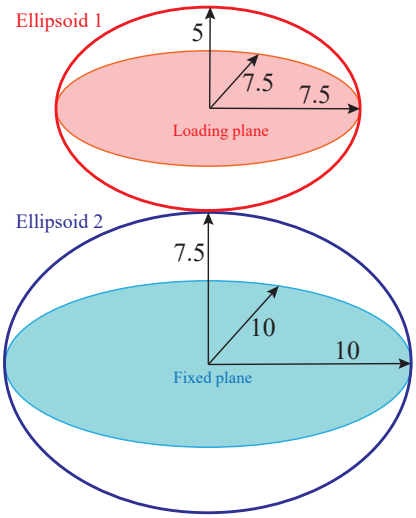

Figure 5: The geometry and loading of the ellipsoid-ellipsoid contact problem (unit:mm).

displayed in Fig. 5, where the loading and constraint conditions similar to the previous two problems are imposed. The numbers of elements for both ellipsoids are 106864 and 244195 respectively, which are in line with the previous two problems. The compressive displacement is taken to be 0.1mm. Again, six test cases corresponding to three different Young's moduli and three Poisson's ratios for the top ellipsoid are numerically simulated. The results are summarised in Table 4. Slightly higher levels of the relative error are obtained in this problem, if comparing cases 1, 2 and 3 with cases 2, 4 and 5 in the sphere-sphere contact problem.

6 Conclusion

Based on the assumptions made in the development of the Hertz contact theory for two linear elastic solids, their strain energy distribution law has been derived, which states that the ratio between the strain energies stored in the two contacting solids is solely dependent on their

Table 4: The material parameters used and comparisons of six ellipsoid-ellipsoid contact cases

Case	E_1 (GPa)	ν_1	S_{e1}^N	S_{e2}^N	S_{e1}^N/S_{e2}^N	S_{e1}/S_{e2}	e_{12}
1	210	0.3	253.4779	262.9316	0.9640	1.0000	-3.6 %
2	105	0.3	227.4210	119.0027	1.9111	2.0000	-4.4 %
3	70	0.3	193.0285	67.6389	2.8538	3.0000	-4.9 %
4	210	0.2	252.7689	247.0227	1.0233	1.0549	-3.0 %
5	210	0.1	251.8711	236.8021	1.0636	1.0879	-2.2 %
6	210	0.0	251.1049	231.4657	1.0848	1.0989	-1.3 %

material properties, regardless of their curvatures in the contact region. The distribution law is generally valid for other contact cases where the Hertz assumptions are largely met. A direct consequence of this law is that the contact point between two particles in DEM could also be determined. The numerical simulations have shown good agreement between the theoretical prediction and the numerical results for the tested cases, although more complex cases have not been considered. The relative errors obtained also indicate that Hertz theory is an approximation.

Acknowledgement

This work is partially supported by the National Natural Science Foundation of China (Grant Nos 51878184 and 51404209). This support is gratefully acknowledged.

References

[1] P. A. Cundall, and O. D. L. Strack. A discrete numerical model for granular assemblies. *Geotechnique*, 29(1):47-65, 1979.

[2] Gang Ma, Yuxiong Zou, Ke Gao, Jidong Zhao, Wei Zhou. Size polydispersity tunes slip avalanches of granular gouge. *Geophysical Research Letters*, 47:e2020GL090458, 2020.

[3] K. J. Johnson. *Contact Mechanics.* Cambridge University Press, 1985.

[4] R. D. Mindlin, H. Deresiewicz. Elastic spheres in contact under varying oblique forces. *Journal of Applied Mechanics.* 20, 327-344, 1953.

[5] Y. T. Feng. An energy-conserving contact theory for discrete element modelling of arbitrarily shaped particles: Basic framework and general contact model. *Comput. Methods Appl. Mech. Engrg.* 2021, 373:113454.

[6] Y. T. Feng. An energy-conserving contact theory for discrete element modelling of arbitrarily shaped discrete elements: Contact volume based model and computational issues. *Comput. Methods Appl. Mech. Engrg.* 2021, 373:113493.

[7] Dassault Systèmes. *ABAQUS Analysis User's Guide 6.14*, Dassault Systèmes Simulia Corporation, DSS Providence, RI, USA, 2014.